Category: BIOLOGICAL SCIENCES Subcategory: MEDICAL SCIENCES

Cardiac electrical defects in progeroid mice and Hutchinson-Gilford progeria syndrome patients with nuclear lamina alterations

Short Title: Cardiac electrical abnormalities in progeria

José Rivera-Torres[a,1], Conrado J. Calvo[a,b,2], Anna Llach[c,2] , Gabriela Guzmán-Martínez[a,d,2], Ricardo Caballero[e], Cristina González-Gómez[a], Luis J. Jiménez-Borreguero[a,f], Juan A. Guadix[g], Fernando G. Osorio[h], Carlos López-Otín[h], Adela Herraiz-Martínez[c,i], Nuria Cabello[i], Alex Vallmitjana[j], Raul Benítez[j], Leslie B. Gordon[k,l], José Jalife[a,m], José Mª Pérez-Pomares[g], Juan Tamargo[e], Eva Delpón[e], Leif Hove-Madsen[c,i], David Filgueiras-Rama[a,n], Vicente Andrés[a,*]

[a] Centro Nacional de Investigaciones Cardiovasculares Carlos III (CNIC), Madrid, Spain.

[b] Grupo Bioingeniería y Electrofisiología Cardíaca GEB, Bio-ITACA, Universitat Politècnica de València, València, Spain.

[c] Institut de Investigació Biomedica Sant Pau, Hospital de Sant Pau, Barcelona, Spain.

[d] Cardiac Imaging Unit, Cardiology Department, Hospital Universitario La Paz, IdiPaz. Madrid, Spain.

[e] Department of Pharmacology, School of Medicine, Universidad Complutense, Madrid, Spain.

[f] Servicio de Cardiología, Hospital de la Princesa, Madrid, Spain.

[g] Department of Animal Biology, Faculty of Science, University of Málaga, Málaga, Spain

[h] Departamento de Bioquímica y Biología Molecular, Instituto Universitario de Oncología (IUOPA), Universidad de Oviedo, Oviedo, Spain.

[i] Cardiovascular Research Center (CSIC-ICCC), Hospital de Sant Pau, Barcelona, Spain.

[j] Automatic Control Department, Universitat Politécnica de Catalunya, Barcelona, Spain.

[k] Department of Pediatrics, Alpert Medical School of Brown University, and Hasbro Children's Hospital, Providence, RI, USA.

[l] Department of Anesthesia, Division of Critical Care Medicine, Boston Children's Hospital and Harvard Medical School, Boston, MA, USA.

[m] Department of Internal Medicine and Center for Arrhythmia Research, University of Michigan, Ann Arbor, MI, USA.

[n] Department of Cardiology. Cardiac Electrophysiology Unit. Hospital Clínico San Carlos. Madrid. Spain.

[1] Present address: Faculty of Biomedical Science, European University of Madrid, Spain

[2] C.J.C., A.L. and G.G.-M. contributed equally to this work.

[3] To whom correspondence should be addressed. Email: vandres@cnic.es.

Character count (with spaces): 40.329 (excluding Title page)

ABSTRACT

Hutchinson-Gilford progeria syndrome (HGPS) is a rare genetic disease caused by defective prelamin-A processing, leading to nuclear lamina alterations, severe cardiovascular pathology, and premature death. Prelamin-A alterations also occur in physiological aging. It remains unknown how defective prelamin-A processing affects the cardiac rhythm. We demonstrate age-dependent cardiac repolarization abnormalities in HGPS patients that are also present in the *Zmpste24*$^{-/-}$ mouse model of HGPS. Challenge of *Zmpste24*$^{-/-}$ mice with the β-adrenergic agonist isoproterenol did not trigger ventricular arrhythmia but caused bradycardia-related premature ventricular complexes and slow-rate polymorphic ventricular rhythms during recovery. Patch-clamping in *Zmpste24*$^{-/-}$ cardiomyocytes revealed prolonged calcium-transient duration and reduced sarcoplasmic reticulum calcium loading and release, consistent with the absence of isoproterenol-induced ventricular arrhythmia. *Zmpste24*$^{-/-}$ progeroid mice also developed severe fibrosis-unrelated bradycardia and PQ interval and QRS complex prolongation. These conduction defects were accompanied by overt mislocalization of the gap-junction protein connexin43 (Cx43). Remarkably, Cx43 mislocalization was also evident in autopsied left ventricle tissue from HGPS patients, suggesting intercellular connectivity alterations at late stages of the disease. The similarities between HGPS patients and progeroid mice reported here strongly suggest that defective cardiac repolarization and cardiomyocyte connectivity are important abnormalities in the HGPS pathogenesis that increase the risk of arrhythmia and premature death.

KEYWORDS: Hutchinson-Gilford progeria syndrome / progerin / prelamin A/ connexin43 / intercellular connectivity / calcium handling / ventricular rhythm.

SIGNIFICANCE

Defective prelamin A processing causes cardiovascular alterations and premature death in HGPS patients, and also occurs during physiological aging. We found overt repolarization abnormalities in HGPS patients at advanced disease stages. Similar alterations were present in progeroid *Zmpste24*$^{-/-}$ mice, whose cardiomyocytes exhibited prolonged calcium transient duration and reduced sarcoplasmic reticulum calcium loading capacity and release, consistent with absence of isoproterenol-induced ventricular arrhythmias. *Zmpste24*$^{-/-}$ mice developed age-dependent bradycardia and PQ interval/QRS complex prolongation, likely contributing to premature death. These defects correlated with mislocalization of connexin43, which was also noted in heart tissue from HGPS patients. These results reveal molecular alterations that might cause cardiac rhythm alterations and premature death in HGPS.

\body

INTRODUCTION

The *LMNA* gene encodes A-type lamins (lamin A and lamin C), key components of the mammalian nuclear envelope with important structural and regulatory functions that affect signaling, transcription, and chromatin organization, among other processes (1). Mature lamin A is produced from the precursor prelamin A through a series of posttranslational modifications, consisting of sequential farnesylation at the cysteine in the CSIM motif, cleavage of the SIM residues, carboxymethylation of the newly accessible cysteine, and a final proteolytic cleavage by the zinc metalloprotease ZMPSTE24/FACE-1 (2).

Mutations in the human *LMNA* gene or defective processing of prelamin A cause a group of diseases termed laminopathies, including the premature aging disorder Hutchinson-Gilford progeria syndrome (HGPS) (OMIM #176670), a very rare genetic disorder with an estimated prevalence of 1 in 21 million people (http://www.progeriaresearch.org/). HGPS patients exhibit accelerated atherosclerosis and arterial stiffness, leading to premature death at an average age of 14.6 years, predominantly from myocardial infarction, heart failure or stroke (3, 4). Most HGPS patients carry a non-inherited *de novo* heterozygous synonymous mutation at codon 608 in *LMNA* (c.1824C>T: GGC>GGT; p.G608G), which activates the use of an internal 5' splicing site in exon 11 that causes the synthesis of progerin. This unprocessed form of prelamin A lacks 50 aminoacids encompassing the ZMPSTE24 cleavage site and therefore remains permanently farnesylated (2). *ZMPSTE24* mutations have also been linked to several other human progeroid syndromes (5, 6), reinforcing the notion that accumulation of progerin or prelamin A accelerates cellular aging. Moreover, progerin and prelamin A are both expressed in cells and tissues of normally aging non-HGPS individuals, suggesting their involvement in physiological aging (reviewed in (2, 7)).

Genetically-modified mice expressing prelamin A or progerin have enabled the study of mechanisms underlying progeria (8) and testing of the efficacy of various therapies (9, 10). Here, we examined cardiac electrical alterations on ECGs of 15 HGPS patients with the classical *LMNA* c.1824C>T mutation, representing approximately 5% of the world population (www.progeriaresearch.org). We then correlated the observed alterations in HGPS patients to the underlying molecular processes in *Zmpste24*-null mice; these mice accumulate farnesylated prelamin A in the nuclear envelope and phenocopy several other defects observed in HGPS, including cardiovascular alterations and premature death (average lifespan ≈20 weeks versus >2 years in wild-type mice) (9, 11).

RESULTS

Electrocardiographic alterations in HGPS patients. Supplemental Tables S1 and **S2** show ECG measurements from HGPS patients carriers of the *LMNA* c.1824C>T mutation (N=15, age range 2-19 years) and controls (N=13, age range 4-19 years), respectively. As they aged, 7 patients showed overt repolarization abnormalities in at least one ECG that were compatible with coronary artery disease (ST depression/elevation, negative and biphasic T waves; representative example in **SI Appendix, Fig.S1A**). One patient showed significant QTc interval prolongation (537 ms) in the context of ischemia at advanced stages of the disease (18 years of age). These ECG alterations were not observed in controls **(**representative example in **SI Appendix, Fig.S1B).** Repolarization abnormalities in HGPS patients were highly evident at advanced disease stages. Compared with age-matched controls, HGPS patients exhibited significant T-wave flattening which was exacerbated as disease progressed (**Fig.1A,** First: initial ECG; Last: last ECG during follow-up). All patients and controls had sinus rhythm and normal PR interval and QRS complex duration **(SI Appendix, Tables S1 and S2).** Interestingly, although all HGPS patients exhibited cardiac rhythm within physiological values, the heart rate and PR interval tended to be slower and larger, respectively, in older HGPS patients (6 out of 15) at the end of the follow-up period (26.8±2.3 months follow-up): heart rate on first and last ECG were 114±7 bpm and 101±7 bpm, respectively, p=0.36; PR on first and last ECG were 115±2 ms and 128±11 ms, respectively, p = 0.22).

Time-course of ECG abnormalities in progeroid *Zmpste24*$^{-/-}$ mice. We next analyzed the electrocardiographic phenotype of *Zmpste24*$^{-/-}$ mice, an established preclinical model of HGPS (9, 11). A glossary of electrocardiographic parameters can be found in the online supplement. To study repolarization, we quantified T-wave flattening by measuring T-wave morphology changes, including sharpness, by excess kurtosis of the T-wave peak in relation to its geometrical change from the isoelectric line and the area under the T wave (see Supplemental Methods). Similarly to HGPS patients, progeroid mice showed repolarization abnormalities manifested as significant T- wave flattening. To determine the risk of ventricular arrhythmia associated with T-wave alterations we used the ß-adrenergic agonist isoproterenol, which can trigger calcium-related alterations in cardiac repolarization. Weekly isoproterenol challenge, based on its sympathomimetic effect and ability to induce Ca^{2+}-related alterations in repolarization, further exacerbated the repolarization alterations as *Zmpste24*$^{-/-}$ mice aged, although acute isoproterenol did not cause significant ventricular arrhythmias in *Zmpste24*$^{-/-}$ or controls **(Fig.1B).** While both groups responded normally in the first week of follow-up, older *Zmpste24*$^{-/-}$ mice developed a very marked reduction in the heart rate (bradycardia) during recovery from isoproterenol **(Fig.2A).** In addition, compared with wild-type controls, *Zmpste24*$^{-/-}$ mice progressively developed longer RR intervals as they aged **(Fig.2B,C).** The variability of the RR interval, measured as the standard deviation (SD-RR), increased linearly as a function of the average RR interval **(SI Appendix, Fig.S2)** and was associated with increased incidence of premature ventricular complexes **(**PVCs, **Fig.2D, and SI Appendix, Fig.S3)** and a short life span. During both isoproterenol challenge **(SI Appendix, Fig.S4)** and recovery **(SI Appendix, Fig.S5)**, *Zmpste24*$^{-/-}$ mice showed increased prolongation of PQ and QRS intervals**.** Progeroid *Zmpste24*$^{-/-}$ mice also developed age-dependent bradycardia in the absence of isoproterenol **(Fig.3A).** In addition, at 18-20 weeks of age, *Zmpste24*$^{-/-}$ mice showed significant signs of defective cardiac conduction compared with

age-matched controls, manifested as prolonged PQ interval and QRS complex, without alterations to the QTc interval **(Fig.3B-E, Supplemental Table S3).**

Preserved cardiac function in *Zmpste24*$^{-/-}$ mice. Transthoracic echocardiography revealed no abnormalities in left ventricle end-diastolic (LVIDs) or end-systolic (LVIDds) parameters in progeroid *Zmpste24*$^{-/-}$ mice **(Fig.3F).** Likewise, *Zmpste24*$^{-/-}$ mice had normal left ventricle mass, posterior wall and interventricular septal thickness at diastole **(SI Appendix, Fig.S6A),** and diastolic function, but had a slightly higher left ventricle ejection fraction (EF) and fractional shortening (FS) than controls **(Fig.3F,** and **SI Appendix, Fig.S6A)**, although within the normal range. The higher ejection fraction in progeriod mice might be explained by bradycardia, since longer diastolic intervals may favor such an increase. In fact, together bradycardia and smaller body surface area in *Zmpste24*$^{-/-}$ mice explain the significantly lower cardiac output compared to wild-type controls **(SI Appendix, Fig.S6B).** However, cardiac index, which relates the cardiac output of the left ventricle per minute to body surface area, was not different between progeroid and wild-type mice **(SI Appendix, Fig.6B).** Time-course studies demonstrated no between-genotype differences in systolic or diastolic blood pressure **(SI Appendix, Fig.S6C).**

***Ex-vivo* cellular electrophysiology.** We next conducted electrophysiology studies in cardiac multicellular preparations from *Zmpste24*$^{-/-}$ mice to identify potential mechanisms underlying the arrhythmia risk associated with abnormal repolarization. No significant between-genotype differences were found in resting membrane potential (RMP), action potential amplitude (APA), maximum velocity of depolarization (V_{max}), or action potential (AP) duration in right or left ventricular samples **(SI Appendix, Table S4).** Moreover, APs recorded in right and left ventricular preparations were indistinguishable between genotypes **(Fig.4A).** Interestingly, most *Zmpste24*$^{-/-}$ ventricular preparations exhibited slow spontaneous automatic activity at ≈3 Hz **(Fig.4B).** Moreover, *Zmpste24*$^{-/-}$ left ventricle preparations displayed after-depolarizations that led to triggered APs, contrasting with normal AP in controls **(Fig.4B, 4C).**

We next analyzed transcription of genes encoding ion channel proteins involved in the different phases of the AP. Real-time qPCR analysis in *Zmpste24*$^{-/-}$ hearts revealed no significant between-group differences in mRNA expression of *Scn5A* (encoding the cardiac sodium channel $Na_V1.5$, involved in cell depolarization) or of *Kcna5*, *Kcnj2*, *Kcnd3*, and *Kcnq1* (respectively encoding the potassium channels $K_v1.5$, Kir2.1, Kv4.3 and Kv7.1, all involved in AP repolarization); in contrast, *Zmpste24*$^{-/-}$ hearts showed significant upregulation of *Kcnh2* (encoding the potassium channel Kv11.1, also known as hERG, involved in AP repolarization) **(SI Appendix, Fig.S7).**

***Zmpste24*$^{-/-}$ mice show defective sarcoplasmic reticulum (SR) Ca^{2+} handling.** We next investigated the role of intracellular Ca^{2+} handling in the observed *in vivo* after-depolarizations and triggered APs in multicellular left ventricle *Zmpste24*$^{-/-}$ preparations. Unlike wild-type cardiomyocytes, *Zmpste24*$^{-/-}$ cardiomyocytes were unable to maintain stable Ca^{2+} transients at higher stimulation frequencies, an effect that was more prominent at 5 mM extracellular Ca^{2+} **(Fig.5A).** To test whether this defect in *Zmpste24*$^{-/-}$ cardiomyocytes was caused by unstable calcium release from the SR through the ryanodine receptor type 2 (RyR2) channel, we measured the frequency of spontaneous calcium waves at rest. However, we found no differences in the calcium wave frequency at any of the calcium concentrations examined **(Fig**

5B). In line with these results, *Zmpste24* deficiency did not affect the transcript level of RyR2 **(Fig.5C),** which is responsible for calcium release from the SR (12).

These findings suggested possible impairment of L-type Ca^{2+} currents (I_{Ca}) or Ca^{2+} uptake by the SR in *Zmpste24*$^{-/-}$ cardiomyocytes as alternative causes for unstable calcium transients. Compared with wild-type controls, *Zmpste24*$^{-/-}$ hearts expressed significantly lower transcript and protein levels of SR Ca^{2+} ATPase (SERCA2a), whereas there was no alteration in transcript levels of *STIM1* and *Orai1*, essential regulators of Ca^{2+} release-activated Ca^{2+} channels **(Fig.5C, 5D).** We also analyzed the expression of calsequestrin 1 (*CSQ1*) and 2 (*CSQ2*), calcium-binding proteins of the SR that help this organelle store a very high amount of Ca^{2+} during relaxation in each contraction-relaxation cycle. Although *CSQ1* and *CSQ2* transcript levels were significantly lower in *Zmpste24*$^{-/-}$ hearts **(Fig.5C)**, no between-genotype differences were observed at the protein level **(Fig.5D).** Likewise, peak I_{Ca} did not differ significantly between cardiomyocytes of the two genotypes **(SI Appendix, Fig.S8).**

To determine SR Ca^{2+} reloading function in ventricular cardiomyocytes, we loaded the SR by exposing cells to an increasing number of stimulation pulses and estimated the resulting Ca^{2+} load from caffeine-elicited inward current traces **(Fig.6A).** SR reloading function was significantly weaker in *Zmpste24*$^{-/-}$ cardiomyocytes than in wild-type cells after 5, 10, and 20 stimulation pulses **(Fig.6B),** and the defective response was still more apparent after ≥30 stimulation pulses **(Fig.6C).** Significantly lower SR Ca^{2+} loading in *Zmpste24*$^{-/-}$ cardiomyocytes was also evident from caffeine-elicited current traces recorded after loading the SR by depolarizing the membrane potential for 5s to -40, -30, -20, or 0 mV **(Fig.6D, 6E).** In addition, intracellular Ca^{2+} transients recorded in isolated cardiomyocytes paced at 0.5 Hz revealed a significantly longer Ca^{2+}-transient duration (at half maximal amplitude) in *Zmpste24*$^{-/-}$ cells **(Fig.6F).**

Finally, we measured the SR Ca^{2+} release-dependent inactivation of the I_{Ca} in response to consecutive stimulation pulses given after clearance of SR Ca^{2+} **(Fig.7A)** in order to assess the feedback of SR calcium release on I_{Ca} inactivation. As expected, current traces recorded in wild-type cardiomyocytes showed a faster rate of I_{Ca} inactivation as the number of pulses used for SR reload increased from 1 (p1) to 30 (p30) **(Fig.7B).** In contrast, the effect of SR loading on the I_{Ca} inactivation rate in *Zmpste24*$^{-/-}$ cardiomyocytes was very modest **(Fig.7B).** Accordingly, the time constant for I_{Ca} inactivation decreased progressively with increasing pulse number in wild-type but not *Zmpste24*$^{-/-}$ cardiomyocytes **(Fig.7C).** Moreover, the amplitude of the intracellular Ca^{2+} transient induced by repeated stimulation at 0.5 Hz was significantly lower in *Zmpste24*$^{-/-}$ cardiomyocytes **(Fig.7D).** Together these findings indicate that SR Ca^{2+} uptake and release are blunted in *Zmpste24*$^{-/-}$ cardiomyocytes, which also explains the failure of acute isoproterenol treatment to induce ventricular arrhythmia despite abnormal repolarization.

Abnormal connexin43 (Cx43) localization in the hearts of *Zmpste24*$^{-/-}$ mice and HGPS patients. To further investigate conduction alterations in progeria, we performed immunohistopathological studies in heart tissue. Cardiomyocyte size was estimated by quantifying their cross-sectional area in heart sections, as well as the membrane capacitance, which is linearly proportional to the plasma membrane area and cell size. Because *Zmpste24*$^{-/-}$

mice are smaller than age-matched controls (9, 11), we normalized results by tibia length. Normalized cross-sectional area and membrane capacitance were similar in cardiomyocytes of both genotypes **(SI Appendix, Fig. S9)**. We also performed Mallory's trichrome staining, which revealed normal chambers, ventricular walls, and myocardial fiber arrangement in *Zmpste24*$^{-/-}$ hearts **(SI Appendix, Fig.S10A, B).** Moreover, Mallory's trichrome staining did not reveal increased fibrosis in the ventricular interstitium **(SI Appendix, Fig.S10B)** or in key structures involved in cardiac conduction such as the atrioventricular node and the main His bundles **(SI Appendix, Fig.S10C),** which might have explained conduction abnormalities in *Zmpste24*$^{-/-}$ mice. However, consistent with previous studies in HGPS patients (13), *Zmpste24*$^{-/-}$ mice showed extensive fibrosis in the tunica media of the major coronary arteries **(SI Appendix, Fig.S11A),** and discontinuous and weak expression of smooth muscle actin within the medial arterial layer **(SI Appendix, Fig.S11B).**

Another possible explanation for the observed cardiac conduction anomalies is altered expression of intercalated disc proteins that play a key role in intercellular connectivity, such as the gap junction protein Cx43 and plakoglobin, as well as cytoskeletal desmosome-interacting proteins such as desmin, a class-III intermediate filament connected to A-type lamins through Nesprin/Sun protein complexes. Western blot analysis in progeroid hearts revealed a significant ≈2-fold increase in Cx43 expression without changes in plakoglobin or desmin **(SI Appendix, Fig.S12).** Remarkably, compared with wild-type controls, *Zmpste24*$^{-/-}$ cardiomyocytes exhibited marked mislocalization of Cx43 to the cytoplasm and the lateral long axis, as revealed by double immunofluorescence to simultaneously detect Cx43 and N-Cadherin **(Fig.8A).** Quantification of digital images revealed less Cx43/N-Cadherin colocalization in the hearts of progeroid mice than in wild-type controls **(Fig. 8E).**

Profound Cx43 mislocalization was also revealed by immunostaining of left ventricle specimens obtained from two HGPS patients at autopsy. In these patients, Cx43 was abundantly associated with the perinuclear rim **(Fig.8B-D),** which is its trafficking origin for subsequent targeting to the intercalated disks (14) (see Discussion). Quantification of digital images confirmed a low percentage of Cx43/N-Cadherin co-localization in HGPS hearts **(Fig.8E).** Defective cardiomyocyte connectivity associated to Cx43 mislocalization may contribute to cardiac conduction defects in progeria (see Discussion).

DISCUSSION

HGPS is a devastating genetic disease resulting from abnormal processing of prelamin-A which is characterized by premature cardiovascular disease and death at an average age of 14.6 years (4). Here, we provide a comprehensive analysis of ECG abnormalities and underlying molecular changes at different stages of HGPS. Our findings may have implications for the risk of premature death in HGPS patients and potentially for normal aging, since defective prelamin A processing has also been revealed in cells and tissues of normally-aging non-HGPS individuals (reviewed in (2, 7)). A previous study identified repolarization abnormalities in 3 out of 15 HGPS patients with the 'classical' *LMNA* c.1824C>T mutation (3). Here, we confirm and extend these findings through a rigorous examination of a new cohort of 15 HGPS patients

carrying the same mutation Half of the patients showed overt repolarization abnormalities in at least one ECG compatible with coronary artery disease (ST depression/elevation, negative and biphasic T waves). Repolarization abnormalities in HGPS patients were strongly evident at advanced disease stages. We also detected prominent mislocalization of Cx43 in left ventricle specimens obtained at autopsy from diseased HGPS patients; Cx43 mislocalization was also observed in the hearts of progeroid *Zmpste24*$^{-/-}$ mice, and is indicative of defective cardiac conduction in progeria (see below).

Animal models resembling the clinical phenotype of HGPS patients are central to understanding the underlying mechanisms of the disease and to developing novel therapies. Our analysis of the well-established *Zmpste24*$^{-/-}$ mouse model of progeria caused by prelamin A accumulation (9, 11) revealed the progressive development of cardiac rhythm alterations that can lead to premature death. *Zmpste24*$^{-/-}$ hearts and cardiomyocytes showed the following specific alterations: i) T-wave repolarization abnormalities, which were also present in half of HGPS patients; ii) prolonged PQ interval and wide QRS complex; iii) development of bradycardia-related premature ventricular complexes and slow-rate polymorphic ventricular rhythms at late disease stages in the absence of ventricular arrhythmias during isoproterenol challenge; iii) automatic spontaneous ventricular activity and after-depolarizations *ex vivo*, which were associated with significantly slowed I_{Ca} inactivation and reduced amplitude of the intracellular Ca^{2+} transient; and iv) mislocalization of Cx43 in the heart.

Notably, some characteristics of the progeroid *Zmpste24*$^{-/-}$ mouse heart are also present in HGPS patients and are frequently observed in normal aging; these include extensive fibrosis and loss of smooth muscle cells in coronary arteries, defective calcium homeostasis, progressive development of repolarization defects, and Cx43 mislocalization (15-17). Overt repolarization abnormalities in ST-T waves and T-wave flattening in mice did not increase the risk of isoproterenol-triggered ventricular arrhythmia. However, T-wave alterations are well known to increase the risk of lethal ventricular arrhythmias during ischemia (18), which might contribute to premature death in HGPS patients from myocardial infarction, one of the main causes of death in this population. T-wave abnormalities might be explained at least in part by an altered repolarization pattern brought about by two opposing ion channel changes observed in the hearts of *Zmpste24*$^{-/-}$ mice: on the one hand, the significant upregulation of *Kcnh2*, which encodes the hERG channel responsible for I_{Kr}, would help terminate the action potential plateau and shorten repolarization (19); on the other hand, the observed slow I_{Ca} inactivation would tend to prolong the plateau and delay repolarization (20). Importantly, an abnormally long QTc interval was observed in only one of 51 ECGs from the 15 HGPS patients, and occurred in the context of ischemia and significant repolarization anomalies. Consistently, we observed no significant QTc prolongation in *Zmpste24*$^{-/-}$ mice, in agreement with the normal APD observed in *Zmpste24*$^{-/-}$ ventricular cardiomyocytes and the majority of ECG traces from HGPS patients. Although we documented significant QRS complex widening in progeroid mice, it is important to note that the high-amplitude QRS complex in the mouse ECG represents not only the spread of depolarization across the ventricle, but also the early phase of repolarization (21). We therefore carefully examined QRS complex and QT duration (QT_{90}, Fig.3B-E) to detect any significant increases in both parameters. However, mouse and human QT intervals must be compared with caution.

The occurrence of bradycardia-related premature ventricular complexes in *Zmpste24*$^{-/-}$ mice during recovery after isoproterenol demonstrates a significant suppression of normal pacemaker activity, with emergence of ventricular ectopic escape discharges. Isoproterenol-induced heart rate increase *in vivo* is associated with increases in intracellular Na^+ and Ca^{2+} concentration (22); these changes, in the presence of the post-isoproterenol-induced bradycardia, likely contributed to the escape discharges and premature ventricular complexes arising from the Purkinje system **(SI Appendix, Fig.S3).** Our *ex-vivo* experiments with multicellular ventricular preparations showed after-depolarizations during spontaneous ventricular activity at ≈3 Hz, which is similar to the cycle length after isoproterenol treatment *in vivo*. Although we were unable to establish the exact origin of these ventricular after-depolarizations, the *in vivo* data support involvement of the Purkinje system, consistent with slow idioventricular discharges (cycle length=266.38, **SI Appendix, Fig.S3**) arising from varying Purkinje locations.

Connexins are the pore-forming subunits of gap junctions and are essential for proper intercellular electrical coupling between cardiomyocytes and for AP spread during each cardiac cycle (23, 24). Cx43 is the major connexin expressed in the ventricles. Its abnormal expression, typically involving downregulation and heterogeneous redistribution to the lateral cardiomyocyte membrane, is associated with different forms of chronic heart disease (hypertrophic, dilated, and ischemic cardiomyopathy) and even with aging (24-26). Defective Cx43 expression results in electrical defects in the myocardium and contributes to arrhythmogenesis. Therefore, Cx43 mislocalization in the heart may explain, at least partly, the prolongation of PQ interval and QRS complex in *Zmpste24*$^{-/-}$ mice. Interestingly, reduced gap junction coupling accompanied by Cx43 lateralization has been linked to reduced functional expression of the alpha subunit ($Na_V1.5$) of the cardiac sodium channel at the intercalated disc (27), and the reduced sodium current is likely to have contributed to the significantly impaired atrioventricular and intraventricular conduction in *Zmpste24*$^{-/-}$ mice. Previous computer simulations (28) suggest that, even in the presence of Cx43 mislocalization and low $Na_V1.5$ expression, a normal peak I_{Ca} with slow inactivation and reduced Ca^{2+} transients could maintain relatively safe conduction in the ventricles of *Zmpste24*$^{-/-}$ mice, albeit at a reduced velocity. However, a high intracellular Ca^{2+} concentration would have compromised propagation safety and caused earlier block, as observed for reduced intercellular coupling (28). Because the intercalated disc is regarded as a functional unit, with gap junction formation requiring the presence of neighboring mechanical junctions (29), we tested the expression of desmin and plakophilin-2. However, our western blot analysis in *Zmpste24*$^{-/-}$ hearts revealed no alterations in the expression of these proteins.

Consistent with the findings in *Zmpste24*$^{-/-}$ mice, immunofluorescence studies in left ventricle specimens from deceased HGPS patients revealed abnormal cellular distribution of Cx43 to a predominantly perinuclear localization. Since Cx43 is packaged into vesicles at the perinuclear trans-Golgi network and is then transported to the intercalated disk (14), our findings suggest that abnormal prelamin A processing causes defective Cx43 targeting to its distinctive microdomain at the gap junctions. Additional *LMNA* mutations might also cause cardiomyopathy by altering connexin expression and/or cellular localization. For example, transgenic mice expressing the lamin A N195K mutant, which causes dilated cardiomyopathy with conduction system disease in humans (DCM-CD1), die at an early age due to arrhythmia, and such a phenotype correlates with cardiac Cx43 and Cx40 misexpression and/or mislocalization (30). Future studies are warranted to elucidate the mechanism causing defective

Cx43 microdomain targeting to gap junctions and their contribution to abnormal cardiac conduction in progeria.

Some of the nuclear envelope alterations in the heart associated with prelamin A or progerin expression also occur during normal aging (15-17), suggesting that shared mechanisms might cause cardiac alterations in HGPS patients and in the geriatric population. Consistent with this idea, prelamin A and progerin are both produced in the cells of normally aging individuals, thus raising the possibility that altered lamin A processing contributes to normal aging and associated cardiovascular disease (reviewed in (2, 7)). Much like in normal human aging, progeroid *Zmpste24*$^{-/-}$ mice develop coronary fibrosis, bradycardia and severe conduction abnormalities. Cardiac conduction abnormalities also arise during aging in wild-type mice, and are associated with an increased incidence of arrhythmias (31). However, Ca^{2+} transients differ between *Zmpste24*$^{-/-}$ mice and normally aging wild-type mice (32), with *Zmpste24*$^{-/-}$ cardiomyocytes being unable to maintain stable Ca^{2+} transients at 4 Hz. Ventricular cardiomyocytes from aged wild-type mice also have a significantly higher incidence of spontaneous Ca^{2+} sparks than cells from young animals; however, we did not observe a similar difference between progeroid mice and age-matched controls. *Zmpste24*$^{-/-}$ mice show weakened I_{Ca} inactivation and defective SR Ca^{2+} uptake and release, features also observed in aging human atrial myocytes (15). In line with this, Ca^{2+} transient amplitudes are reduced in progeroid mice **(Fig.6)**, in aged wild-type mice (32), and in aged human atrial cardiomyocytes (15).

The progressively developing bradycardia and deteriorating cardiac conduction in progeriod mice also resemble clinical rhythm abnormalities observed in the elderly (16, 17). Although the commonest age-related cardiac conduction abnormality in humans is degenerative fibrosis (33), *Zmpste24*$^{-/-}$ mice did not show abnormal fibrosis in the ventricular interstitium or in the major conduction structures. However, in line with observations in HGPS patients (13), the coronary arteries of *Zmpste24*$^{-/-}$ mice showed extensive fibrosis and reduced accumulation of smooth muscle cells, potential causes of vascular stiffening, reduced coronary flow, and abnormal impulse generation in the sinoatrial node and conduction in the atria and ventricles. The latter may have also contributed to T-wave alterations, especially during isoproterenol challenge, as well as to progressive development of bradycardia in progeroid *Zmpste24*$^{-/-}$ mice. In fact, human patients with coronary artery disease show a high prevalence of conduction abnormalities such as atrioventricular or sinoatrial block (34).

Study Limitations. We provide a comprehensive characterization of cardiac abnormalities in HGPS patients and progeroid *Zmpste24*$^{-/-}$ mice, identifying a number of cellular and molecular alterations in both species that are likely to contribute to defective cardiac repolarization and conduction in progeria. Future studies are warranted to establish direct causal connections between the presence of unprocessed prelamin A or progerin and the cardiac abnormalities associated with HGPS with the goal of identifying novel targets for therapeutic intervention. Based on our findings, major efforts should be placed into elucidating the mechanisms causing Cx43 mislocalization in the heart of progeroid mice and HGPS patients. These studies may pave the way to developing efficient therapies to improve cardiac conduction in progeria.

Although ion channels are highly conserved between humans and mice, significant electrophysiological differences exist (35), making it difficult to translate mouse findings to the

clinical arena. For example, although we observed a tendency toward a slower heart rate in older HGPS patients with longer follow-up, HGPS patients did not show the bradycardia and other conduction abnormalities that appeared progressively in *Zmpste24*$^{-/-}$ mice. This might have been due to the lack of sequential ECG assessment in humans until very advanced disease stage. Indeed, human left ventricle specimens obtained by autopsy revealed reduced localization of Cx43 at gap junctions, consistent with altered ventricular conduction velocity.

Continuous telemetry and other invasive electrophysiological measurements would have been desirable in *Zmpste24*$^{-/-}$ mice. However, these animals show severe body weight loss (body weight ≈9 g at late stages compared with ≈30 g in age-matched wild-type controls) and are physically extremely fragile, precluding the use of commercially available telemetry systems or any other invasive approaches to register specific arrhythmias forecasting premature death. The physical deterioration of HGPS patients also limits implementation of any invasive measurements (e.g., implantable loop recordings) to further study rhythm abnormalities.

MATERIALS AND METHODS

Clinical information from children with HGPS was obtained from The Progeria Research Foundation Medical and Research Database (PI L.B.G.), and approved by the Rhode Island Hospital and Brown University Institutional Review Boards (Providence, RI). All participants or parents provided written informed consent in the primary language of the participant or parent. When appropriate, interpreters were used for consenting. At least one ECG recorded no more than 3 years before death was obtained from each of 15 HGPS patients. Thirteen gender and age-matched control volunteers were weighed and ECG traces recorded for comparison. All control volunteers or parents provided written informed consent. Animal studies were carried out in male *Zmpste24*$^{-/-}$ mice (11) and age-matched wild-type male littermates (all C57BL/6). Animals were reared and housed in accordance with institutional guidelines and regulations. All other detailed materials and methods are described in the SI Materials and Methods.

ACKNOWLEDGEMENTS

We thank María Jesús Andrés for technical assistance and help with art work, Susan Campbell for assistance with patient information, Maite Dubraska for assistance with blood sampling and ECG in control subjects, Inés Ortega and Virginia Zorita for animal maintenance and care, and Simon Bartlett for English editing. This work was supported by the Spanish Ministry of Economy and Competitiveness (MINECO) (grants SAF2010-16044, SAF2011-30312, SAF2011-30088, SAF2013-46663-R, SAF2014-52413-R) and Fondo de Investigación Sanitaria del Instituto de Salud Carlos III (grants RD12/0042/0028, RD12/0042/0011, RD12/0042/0002) with co-funding from the Fondo Europeo de Desarrollo Regional (FEDER), and The Progeria Research Foundation. JAG is the recipient of Marie Curie COFUND U-Mobility Grant No.246550. The Instituto Universitario de Oncología is supported by Obra Social Cajastur. The CNIC is supported by the MINECO and the Pro CNIC Foundation, and is a Severo Ochoa Center of Excellence (MINECO award SEV-2015-0505).

AUTHOR CONTRIBUTION

- J.R.-T., D.F.-R., J.J., R.C., E.D., J.T., L.H.-M. and V.A. designed research.
- J.R.-T., G.G.-M., C.J.C., L.J.J.-B., J.M.P.-P., R.C., E.D., J.T., L.B.G, F.G.O., L.H.-M., D.F.-R., and V.A. analyzed data.
- J.R.-T., A.L., G.G.-M., R.C., C.J.C., C.G.-G., L.J.J.-B., J.A.G., A.H., N.C., A.V., R.B., J.M.P.-P., J.T., E.D., and L.H.-M. performed research.
- J.R.-T., C.G.-G., F.G.O., and C.L-O. generated and maintained mice and cells.
- J.R.-T., D.F.-R., J.J., C.L.-O., C.J.C., E.D., L.B.G., L.H.-M. and V.A. wrote the paper.

CONFLICT OF INTEREST

None to declare.

REFERENCES

1. Andrés V & González JM (2009) Role of A-type lamins in signaling, transcription, and chromatin organization. *J Cell Biol* 187(7):945-957.
2. Trigueros-Motos L, González JM, Rivera J, & Andrés V (2011) Hutchinson-Gilford progeria syndrome, cardiovascular disease and oxidative stress. *Front Biosci* 3:1285-1297.
3. Merideth MA*, et al.* (2008) Phenotype and course of Hutchinson-Gilford progeria syndrome. *New Engl J Med* 358(6):592-604.
4. Gordon LB*, et al.* (2014) Impact of farnesylation inhibitors on survival in Hutchinson-Gilford progeria syndrome. *Circulation* 130(1):27-34.
5. Barrowman J, Wiley PA, Hudon-Miller SE, Hrycyna CA, & Michaelis S (2012) Human ZMPSTE24 disease mutations: residual proteolytic activity correlates with disease severity. *Hum Mol Gen* 21(18):4084-4093.
6. Osorio FG*, et al.* (2011) Cell autonomous and systemic factors in progeria development. *Biochem Soc Trans* 39(6):1710-1714.
7. Gordon LB, Rothman FG, Lopez-Otin C, & Misteli T (2014) Progeria: a paradigm for translational medicine. *Cell* 156(3):400-407.
8. Zhang H, Kieckhaefer JE, & Cao K (2013) Mouse models of laminopathies. *Aging Cell* 12(1):2-10.
9. Varela I*, et al.* (2005) Accelerated ageing in mice deficient in Zmpste24 protease is linked to p53 signalling activation. *Nature* 437(7058):564-568.
10. Villa-Bellosta R*, et al.* (2013) Defective extracellular pyrophosphate metabolism promotes vascular calcification in a mouse model of Hutchinson-Gilford progeria syndrome that is ameliorated on pyrophosphate treatment. *Circulation* 127(24):2442-2451.
11. Pendas AM*, et al.* (2002) Defective prelamin A processing and muscular and adipocyte alterations in Zmpste24 metalloproteinase-deficient mice. *Nat Gen* 31(1):94-99.
12. Willis BC*, et al.* (2016) Constitutive Intracellular Na+ Excess in Purkinje Cells Promotes Arrhythmogenesis at Lower Levels of Stress Than Ventricular Myocytes From Mice With Catecholaminergic Polymorphic Ventricular Tachycardia. *Circulation* 133(24):2348-2359.
13. Olive M*, et al.* (2010) Cardiovascular pathology in Hutchinson-Gilford progeria: correlation with the vascular pathology of aging. *Arterioscl Thromb Vasc Biol* 30(11):2301-2309.
14. Smyth JW*, et al.* (2012) Actin cytoskeleton rest stops regulate anterograde traffic of connexin 43 vesicles to the plasma membrane. *Cir Res* 110(7):978-989.
15. Herraiz-Martinez A*, et al.* (2015) Ageing is associated with deterioration of calcium homeostasis in isolated human right atrial myocytes. *Cardiovasc Res* 106(1):76-86.
16. Jensen PN*, et al.* (2014) Incidence of and risk factors for sick sinus syndrome in the general population. *J Am Coll Cardiol* 64(6):531-538.
17. Strait JB & Lakatta EG (2012) Aging-associated cardiovascular changes and their relationship to heart failure. *Heart Fail Clin* 8(1):143-164.
18. Verrier RL & Ikeda T (2013) Ambulatory ECG-based T-wave alternans monitoring for risk assessment and guiding medical therapy: mechanisms and clinical applications. *Prog Cardiovasc Dis* 56(2):172-185.

19. Perry M, Sanguinetti M, & Mitcheson J (2010) Revealing the structural basis of action of hERG potassium channel activators and blockers. *J Physiol* 588(Pt 17):3157-3167.
20. Madhvani RV*, et al.* (2015) Targeting the late component of the cardiac L-type Ca2+ current to suppress early afterdepolarizations. *J Gen Physiol* 145(5):395-404.
21. Mitchell GF, Jeron A, & Koren G (1998) Measurement of heart rate and Q-T interval in the conscious mouse. *The American journal of physiology* 274(3 Pt 2):H747-751.
22. Vassalle M (1977) The relationship among cardiac pacemakers. Overdrive suppression. *Circ Res* 41(3):269-277.
23. Vaidya D*, et al.* (2001) Null mutation of connexin43 causes slow propagation of ventricular activation in the late stages of mouse embryonic development. *Circ Res* 88(11):1196-1202.
24. Fontes MS, van Veen TA, de Bakker JM, & van Rijen HV (2012) Functional consequences of abnormal Cx43 expression in the heart. *Biochim Biophys Acta* 1818(8):2020-2029.
25. Peters NS (1996) New insights into myocardial arrhythmogenesis: distribution of gap-junctional coupling in normal, ischaemic and hypertrophied human hearts. *Clin Sci (Lond)* 90(6):447-452.
26. Saffitz JE, Schuessler RB, & Yamada KA (1999) Mechanisms of remodeling of gap junction distributions and the development of anatomic substrates of arrhythmias. *Cardiovasc Res* 42(2):309-317.
27. Cerrone M*, et al.* (2012) Sodium current deficit and arrhythmogenesis in a murine model of plakophilin-2 haploinsufficiency. *Cardiovasc Res* 95(4):460-468.
28. Shaw RM & Rudy Y (1997) Ionic mechanisms of propagation in cardiac tissue. Roles of the sodium and L-type calcium currents during reduced excitability and decreased gap junction coupling. *Circ Res* 81(5):727-741.
29. Delmar M & McKenna WJ (2010) The cardiac desmosome and arrhythmogenic cardiomyopathies: from gene to disease. *Circ Res* 107(6):700-714.
30. Mounkes LC, Kozlov SV, Rottman JN, & Stewart CL (2005) Expression of an LMNA-N195K variant of A-type lamins results in cardiac conduction defects and death in mice. *Hum Mol Genet* 14(15):2167-2180.
31. Signore S*, et al.* (2015) Late Na(+) current and protracted electrical recovery are critical determinants of the aging myopathy. *Nat Commun* 6:8803.
32. Howlett SE, Grandy SA, & Ferrier GR (2006) Calcium spark properties in ventricular myocytes are altered in aged mice. *Am J Physiol Heart Circ Physiol* 290(4):H1566-1574.
33. Ferrer MI (1982) The etiology and natural history of sinus node disorders. *Arch Intern Med* 142(2):371-372.
34. Hsueh CW, Lee WL, Chen YT, & Ting CT (2001) The incidence of coronary artery disease in patients with symptomatic bradyarrhythmias. *Jpn Heart J* 42(4):417-423.
35. London B (2001) Cardiac arrhythmias: from (transgenic) mice to men. *J Cardiovasc Electrophysiol* 12(9):1089-1091.

FIGURE LEGENDS

FIGURE 1. Age-related exacerbation of repolarization abnormalities in HGPS patients and *Zmpste24*$^{-/-}$ *mice*. (A) Left: Extracted averaged ECG leads II and V5 from human control participants (blue traces) and HGPS patients at initial stage ('First', light red trace) and in advanced stages ('Last', dark red trace). **Right:** Quantification of mean flattening scores. **(B) Left:** Representative T-wave abnormalities in *Zmpste24*$^{-/-}$ mice, comparing the first and the last isoproterenol (ISO) challenge (First: 11-week-old; Last: 19-week-old or last week before death; see Supplementary Methods). **Right:** Mean effective flattening scores at baseline, after ISO exposure and during 5 min recovery. *, $p<0.05$ vs control; †, $p<0.05$ vs First follow up.

FIGURE 2. Severe bradycardia in post-isoproterenol administration recovery is associated with an increase in premature ventricular complexes in *Zmpste24*$^{-/-}$ mice. (A) β-adrenergic response (interbeat interval, IBI) in wild-type and *Zmpste24*$^{-/-}$ mice from the first to the last isoproterenol challenge (ISO) (First: 11-week-old; Last: 19-week-old or last week before death. **(B)** RR histograms and RRn/RRn+1 correlation plots in wild-type and *Zmpste24*$^{-/-}$ mice during ISO time-course challenge (color-coded time scale). A significant increase in the percentage of long RR intervals during the last week of follow up **(C)** was also associated with a significant increase in bradycardia-related premature ventricular complexes. **(D)** First: 11-week-old; Last; 19-week-old or last week before death. See SI Materials and Methods. *, $p<0.05$; **, $p<0.01$.

FIGURE 3. *Zmpste24*$^{-/-}$ mice show preserved cardiac function but develop severe bradycardia and cardiac conduction abnormalities. (A) Heart rate (bpm, beats per minute) in conscious mice. **(B)** Template ECG showing the intervals used to quantify **(C)** PQ, **(D)** QRS and **(E)** heart-rate-corrected QT at 90% of repolarization from T_{peak} (QTc_{90}) duration, measured on the baseline ECG at the first follow-up (week 11; First) and at the last follow-up (Last; see Supplementary Methods). **(F)** Left ventricular internal diameter (LVID) at systole (s) and diastole (d) and ejection fraction (EF) determined by trans-thoracic echocardiography in 18-20-week-old mice. *, $p<0.05$; **, $p<0.01$; ***, $p<0.001$.

FIGURE 4. Transmembrane action potentials recorded in multicellular left ventricular preparations. (A) Representative APs (3 Hz) from wild-type and *Zmpste24*$^{-/-}$ mice. **(B)** Left ventricular preparations from *Zmpste24*$^{-/-}$ mice displayed after-depolarizations that occasionally yielded triggered APs (C, bottom).

FIGURE 5. Defective Ca^{2+} transients in *Zmpste24*$^{-/-}$ cardiomyocytes. (A) Left: Analysis of beat-to-beat response stability in isolated mouse ventricular myocytes subjected to increasing stimulation frequencies. Representative examples of calcium transients recorded in the presence of 5 mM extracellular $Ca^{2+}$are shown. Irregular beat-to-beat responses start at lower frequencies in *Zmpste24*$^{-/-}$ cardiomyocytes. **Right:** The graph shows threshold frequencies (in Hz) for the induction of non-uniform beat-to-beat responses at the indicated Ca^{2+} concentrations. Responses were recorded in myocytes isolated from wild-type and *Zmpste24*$^{-/-}$ mice (12 cells from 6 mice of each genotype). **(B) Top:** Typical recordings of spontaneous calcium waves at the indicated Ca^{2+} concentrations. **Bottom:** Calcium dependency of the calcium wave frequency. Values are from 7 wild-type mice (n=15 cells) and 6 *Zmpste24*$^{-/-}$ mice (n=14 cells) **(C)** qPCR of heart tissue. **(D)** Western blot analysis of heart tissue. Representative

blots are shown and relative band intensity was quantified as described in Supplemental Methods. *, $p<0.05$; **, $p<0.01$; ***, $p<0.001$.

FIGURE 6. Reduced maximal sarcoplasmic reticulum Ca^{2+} uptake in *Zmpste24*$^{-/-}$ cardiomyocytes. SR calcium loading capacity in isolated ventricular myocytes. **(A-C)** Calcium loading measured as a function of the number of stimulation pulses used for SR loading. **(A)** Representative caffeine-induced currents recorded after SR reloading with the indicated number of stimulation pulses (p). Transient exposure to caffeine (CAF) was used to release SR calcium content before reloading and to measure loading after the train of stimulation pulses. **(B)** Time integral of caffeine-induced currents recorded after SR reloading with the indicated stimulation pulses. Data were obtained from 7 *Zmpste24*$^{-/-}$ and 8 wild-type myocytes (from n=5 mice) exposed consecutively to 2 and 5 mM extracellular Ca^{2+}. Time integrals were converted to amoles and normalized to cellular capacitance (in pF). **(C)** Effect of extracellular calcium concentration on the time integral of caffeine-induced current at steady-state (after ≥30 stimulation pulses). **(D-F)** Calcium loading measured as a function of membrane potential. **(D)** Representative caffeine-induced currents recorded after SR loading with a 5s depolarization to the indicated membrane potentials. **(E)** Time integral of caffeine-induced current recorded in the presence of 2 mM extracellular Ca^{2+} after SR reloading at rest (-80 mV) and after depolarizing to the indicated voltage. Data were obtained from 8 *Zmpste24*$^{-/-}$ myocytes (n=5 mice) and 9 wild-type myocytes (n=6 mice). **(F)** Mean calcium transient duration at half maximal amplitude (DHMA) recorded in myocytes paced at 0.5 Hz (17 wild-type and 18 *Zmpste24*$^{-/-}$ myocytes from n=6 mice per group). *, $p< 0.05$.

FIGURE 7. Impaired sarcoplasmic reticulum calcium release-dependent inactivation of L-type calcium currents in isolated *Zmpste24*$^{-/-}$ myocytes. (A) Protocol to measure the effect of SR calcium loading on I_{Ca} inactivation. SR calcium content was released with caffeine (CAF) and reloaded with a train of stimulation pulses (p). **(B)** Representative superimposed I_{Ca} recordings on p1 and p30. Currents were normalized to their peak values and fitted to a double exponential equation. **(C)** Dependency of time constant (tau) for fast I_{Ca} inactivation on indicated pulses. **(D)** Representative calcium transient ($\Delta F/F0$) recordings from myocytes paced at 0.5 Hz (left) and calcium transient amplitude quantification (right). Indicated cardiomyocytes are from n=6 mice/genotype. *, $p<0.05$; **, $p<0.01$; ***, $p<0.001$.

FIGURE 8. Abnormal localization of connexin43 in hearts of progeroid Zmpste24-/- mice and HGPS patients. (A, B) Double immunofluorescence of left ventricle sections from mice of the indicated gentoype and HGPS patients to detect N-Cadherin (N-Cadh, Left panels: green) and Cx43 (Middle panels: red). Right panels show merged images, with DAPI staining of nuclei (blue). **(A)** Cx43 lateralization was evident in *Zmpste24*$^{-/-}$ mice. Green arrows mark examples of intercalated disk areas (N-Cadh-positive). The white arrow in the *Zmpste24*$^{-/-}$ image marks an intercalated disk without Cx43 expression, and the red arrow in the wild-type image marks an intercalated disk with abundant Cx43 expression. **(B)** Representative images illustrating loss of Cx43/N-Cadh colocalization in HGPS heart. Green and white arrows are as in panel A. The red arrow marks a Cx43 positive area which does not colocalize with N-Cadh. **(C)** Zoom-in of a HGPS heart section showing predominat Cx43 expression near the nuclei and scarce Cx43/N-Cadh colocalization at the intercalated disks. **(D)** Automatic image segmentation of a HGPS heart section used for quantification of Cx43/N-Cadh colocalization. Green, red and dark-blue blob boundaries correspond to positive staining for N-Cadh, Cx43,

and nuclei, respectively. Cyan blob-boundaries represent areas showing Cx43/nuclei colocalization. **(E)** Percentage of Cx43/N-Cadh colocalization at the intercalated disks estimated by quantifying automatically-segmented images. Results are represented relative to wild-type (=100). N=3 wild-type and *Zmpste24*$^{-/-}$ mice, and N=2 HGPS patients were analyzed (n=5 sections per individual). *, $p<0.001$. White bars in the photomicrographs represent 50 μm.

FIGURE 1

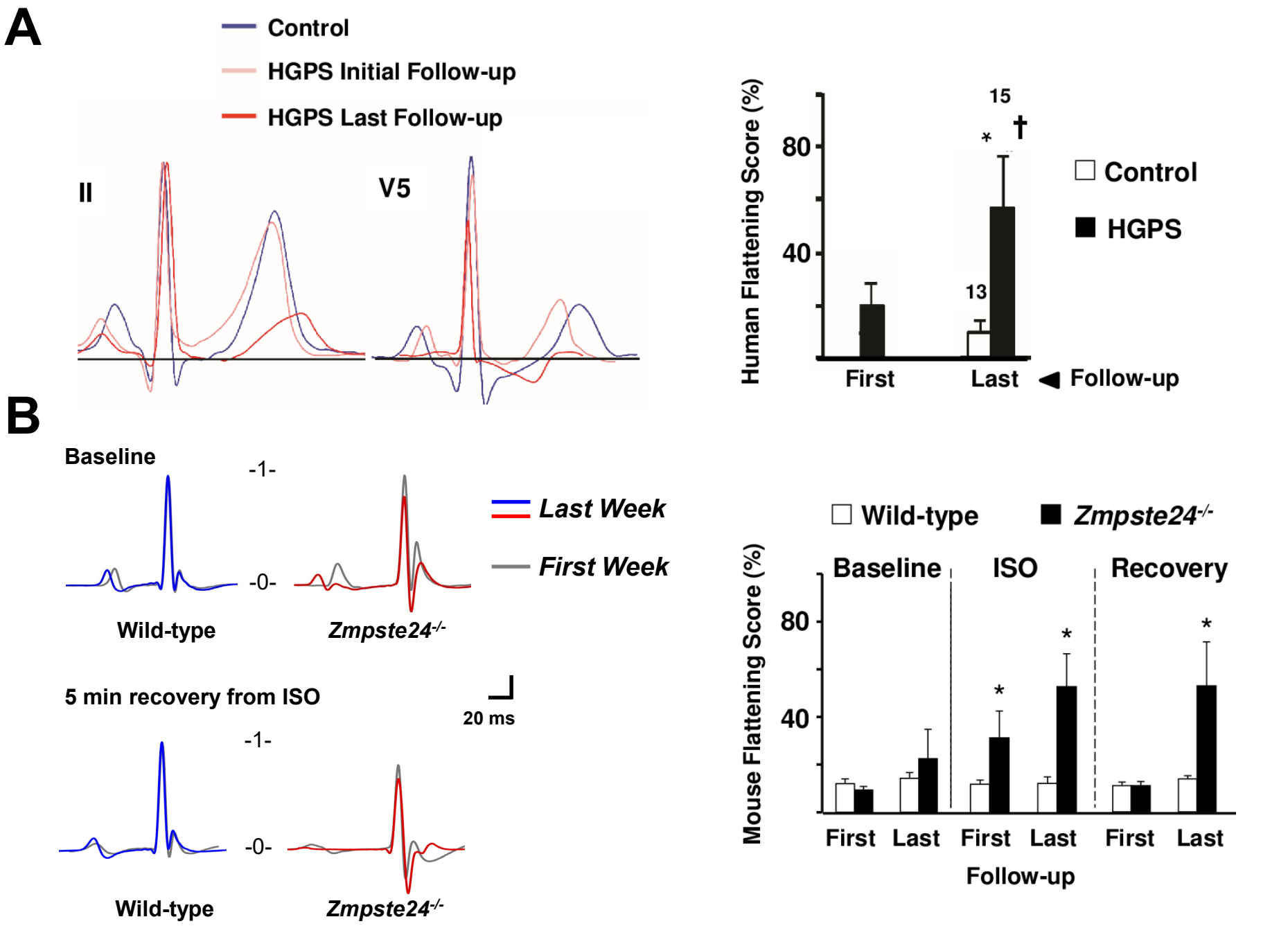
A
Control
HGPS Initial Follow-up
HGPS Last Follow-up
II
V5
Human Flattening Score (%)
80
40
15
*
†
13
Control
HGPS
First
Last
Follow-up
B
Baseline
-1-
-0-
Last Week
First Week
Wild-type
Zmpste24-/-
5 min recovery from ISO
20 ms
-1-
-0-
Wild-type
Zmpste24-/-
Wild-type
Zmpste24-/-
Mouse Flattening Score (%)
Baseline
ISO
Recovery
80
40
*
*
*
First
Last
First
Last
First
Last
Follow-up

FIGURE 2

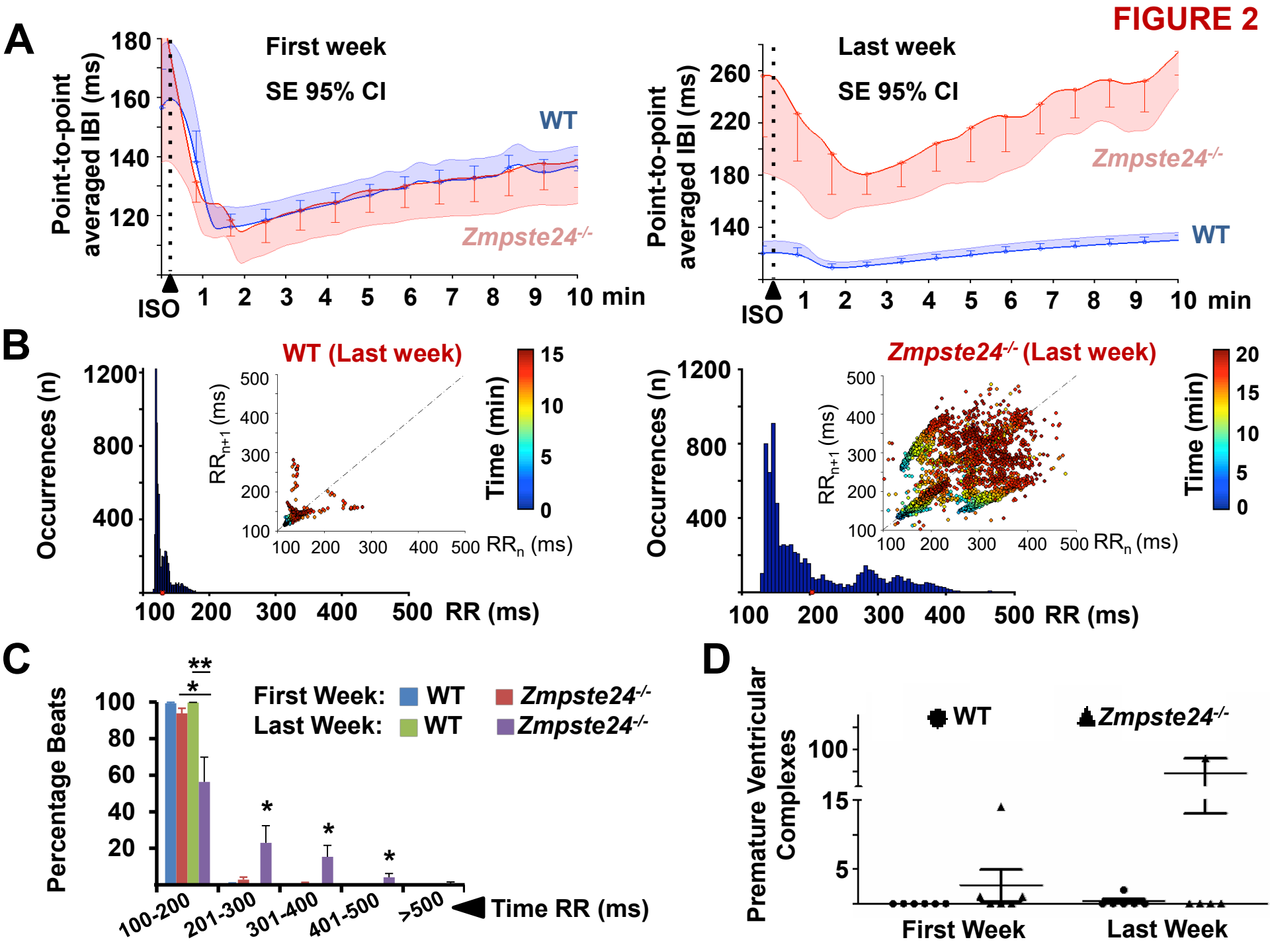
A
First week
SE 95% CI
WT
Zmpste24-/-
Point-to-point averaged IBI (ms)
ISO
1 2 3 4 5 6 7 8 9 10 min
Last week
SE 95% CI
Zmpste24-/-
WT
B
WT (Last week)
Zmpste24-/- (Last week)
Occurrences (n)
RRn+1 (ms)
RRn (ms)
Time (min)
RR (ms)
C
Percentage Beats
First Week: WT Zmpste24-/-
Last Week: WT Zmpste24-/-
100-200
201-300
301-400
401-500
>500
Time RR (ms)
D
Premature Ventricular Complexes
WT
Zmpste24-/-
First Week
Last Week

FIGURE 3

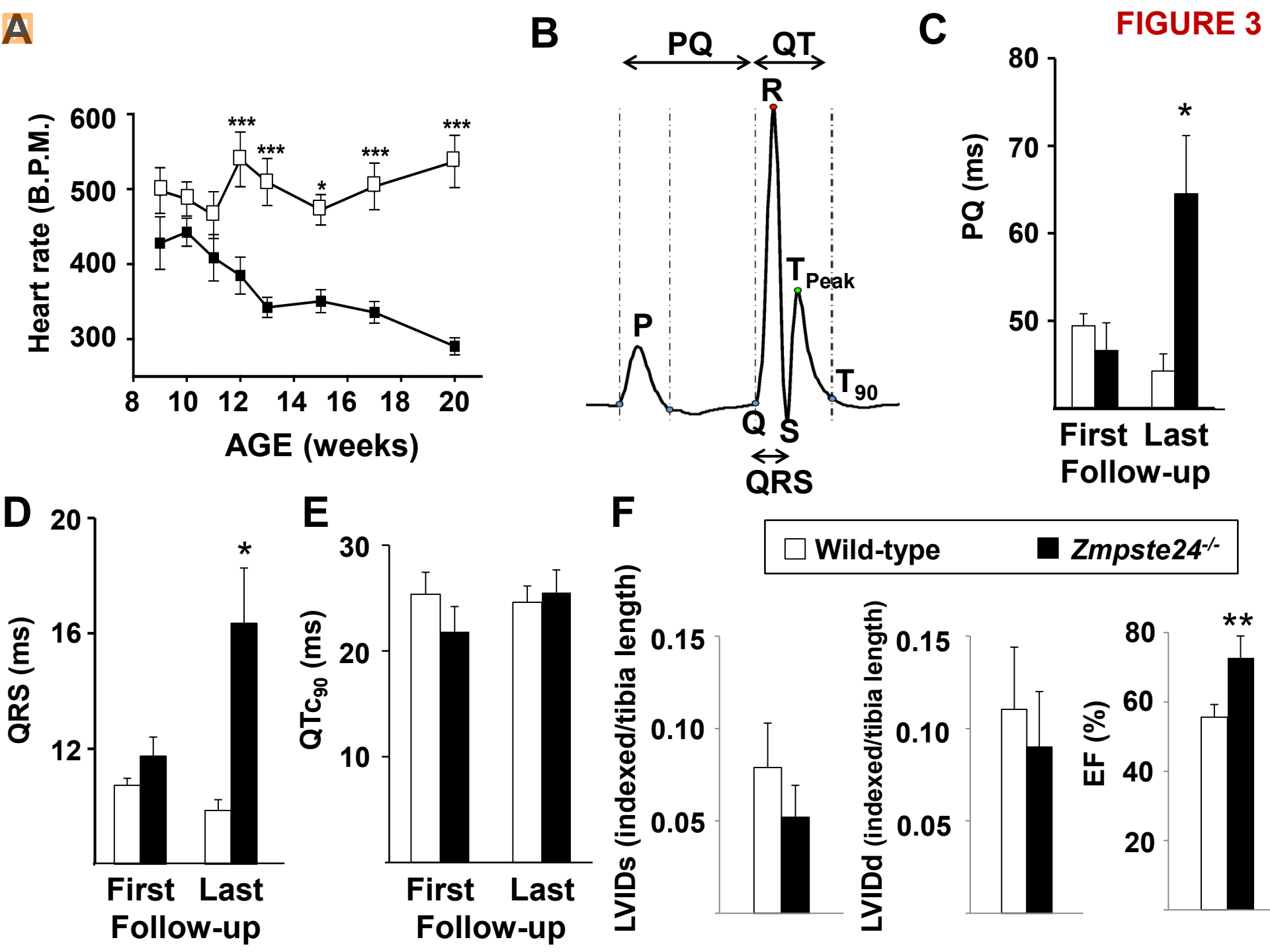
A
Heart rate (B.P.M.)
600
500
400
300
***
***
*
***
***
8
10
12
14
16
18
20
AGE (weeks)
B
PQ
QT
R
P
T Peak
T90
Q
S
QRS
C
PQ (ms)
80
70
60
50
*
First
Last
Follow-up
D
QRS (ms)
20
16
12
*
First
Last
Follow-up
E
QTc90 (ms)
30
20
10
First
Last
Follow-up
F
Wild-type
Zmpste24-/-
LVIDs (indexed/tibia length)
0.15
0.10
0.05
LVIDd (indexed/tibia length)
0.15
0.10
0.05
EF (%)
80
60
40
20
**

FIGURE 4

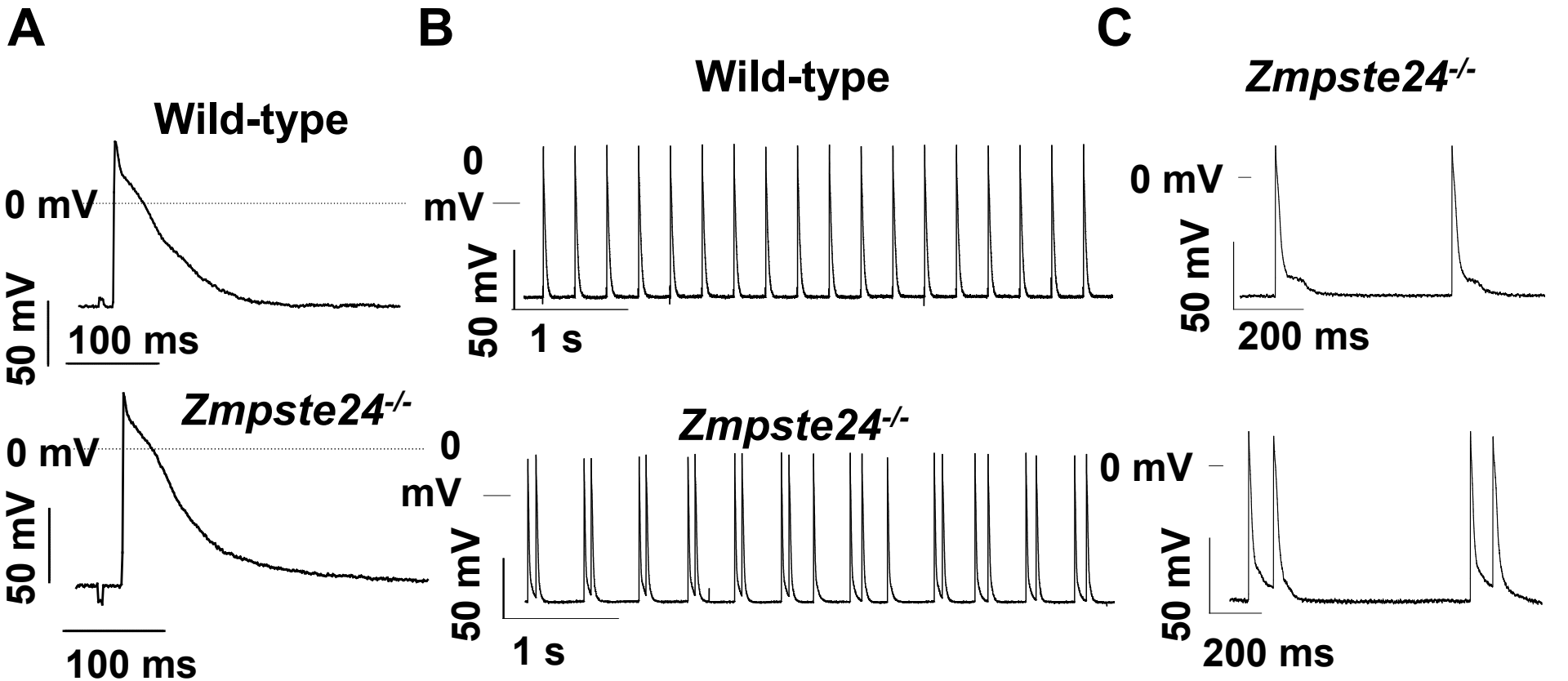
A
Wild-type
0 mV
50 mV
100 ms
Zmpste24-/-
0 mV
50 mV
100 ms
B
Wild-type
0 mV
50 mV
1 s
Zmpste24-/-
0 mV
50 mV
1 s
C
Zmpste24-/-
0 mV
50 mV
200 ms
0 mV
50 mV
200 ms

FIGURE 5

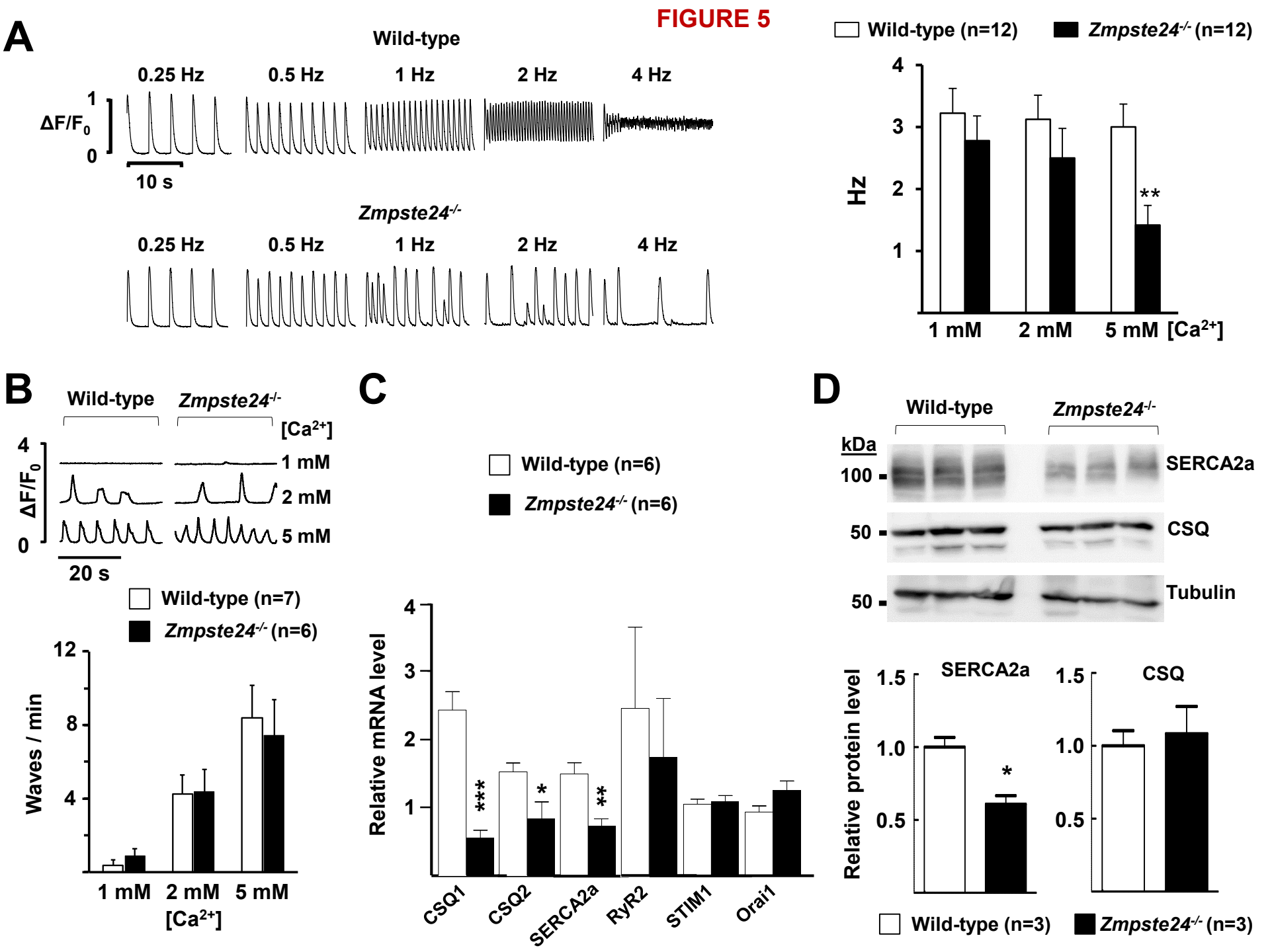
A
Wild-type
0.25 Hz
0.5 Hz
1 Hz
2 Hz
4 Hz
ΔF/F0
1
0
10 s
Zmpste24-/-
0.25 Hz
0.5 Hz
1 Hz
2 Hz
4 Hz
Wild-type (n=12)
Zmpste24-/- (n=12)
Hz
4
3
2
1
**
1 mM
2 mM
5 mM [Ca2+]
B
Wild-type
Zmpste24-/-
[Ca2+]
4
ΔF/F0
0
1 mM
2 mM
5 mM
20 s
Wild-type (n=7)
Zmpste24-/- (n=6)
Waves / min
12
8
4
1 mM
2 mM
5 mM
[Ca2+]
C
Wild-type (n=6)
Zmpste24-/- (n=6)
Relative mRNA level
4
3
2
1
***
*
**
CSQ1
CSQ2
SERCA2a
RyR2
STIM1
Orai1
D
Wild-type
Zmpste24-/-
kDa
100
50
50
SERCA2a
CSQ
Tubulin
Relative protein level
SERCA2a
1.5
1.0
0.5
*
CSQ
1.5
1.0
0.5
Wild-type (n=3)
Zmpste24-/- (n=3)

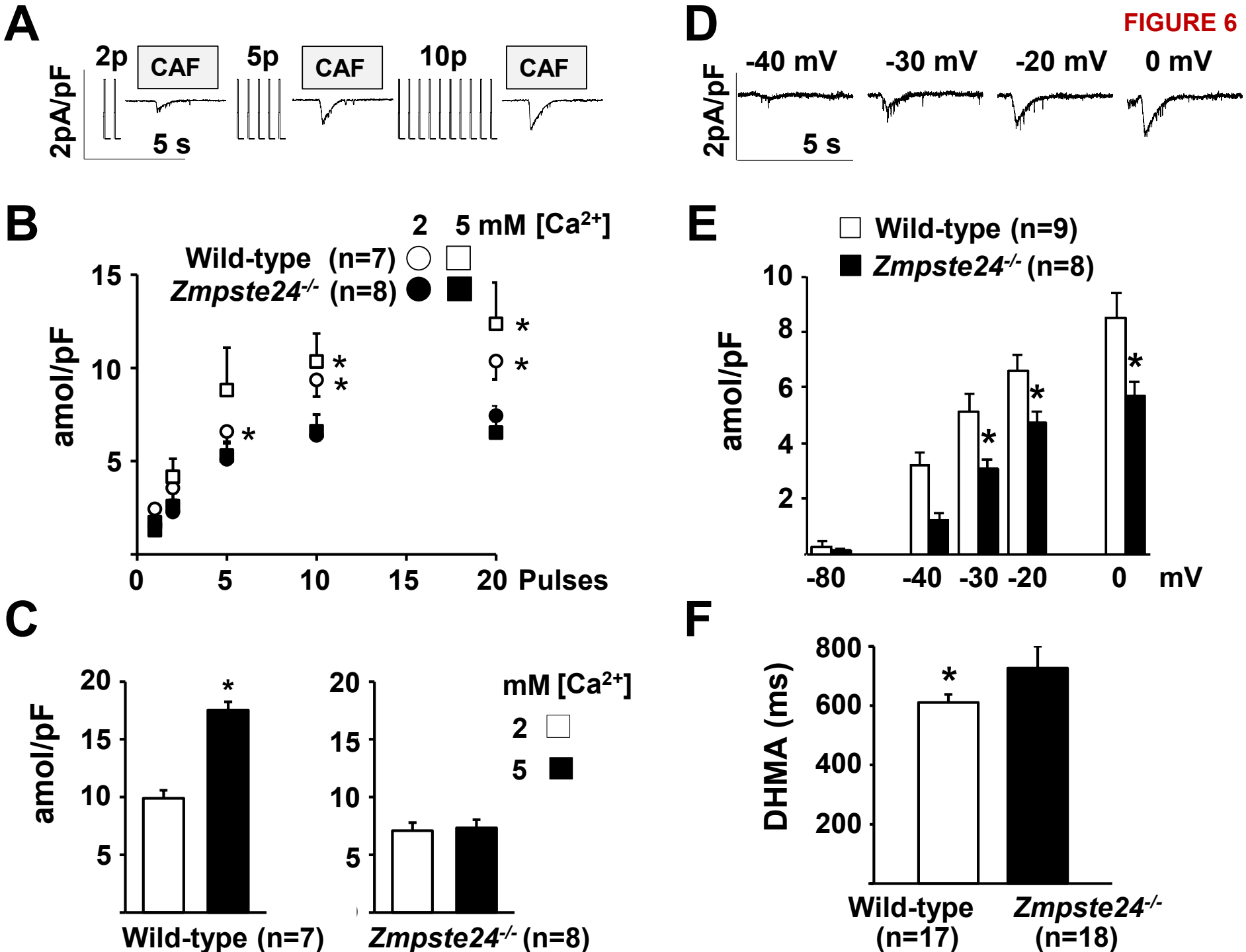
A
2p
CAF
5p
CAF
10p
CAF
2pA/pF
5 s
D
-40 mV
-30 mV
-20 mV
0 mV
2pA/pF
5 s
B
2
5 mM [Ca2+]
Wild-type (n=7)
Zmpste24-/- (n=8)
amol/pF
15
10
5
0
5
10
15
20 Pulses
E
Wild-type (n=9)
Zmpste24-/- (n=8)
amol/pF
10
8
6
4
2
-80
-40
-30
-20
0
mV
C
amol/pF
20
15
10
5
Wild-type (n=7)
Zmpste24-/- (n=8)
mM [Ca2+]
2
5
F
DHMA (ms)
800
600
400
200
Wild-type (n=17)
Zmpste24-/- (n=18)

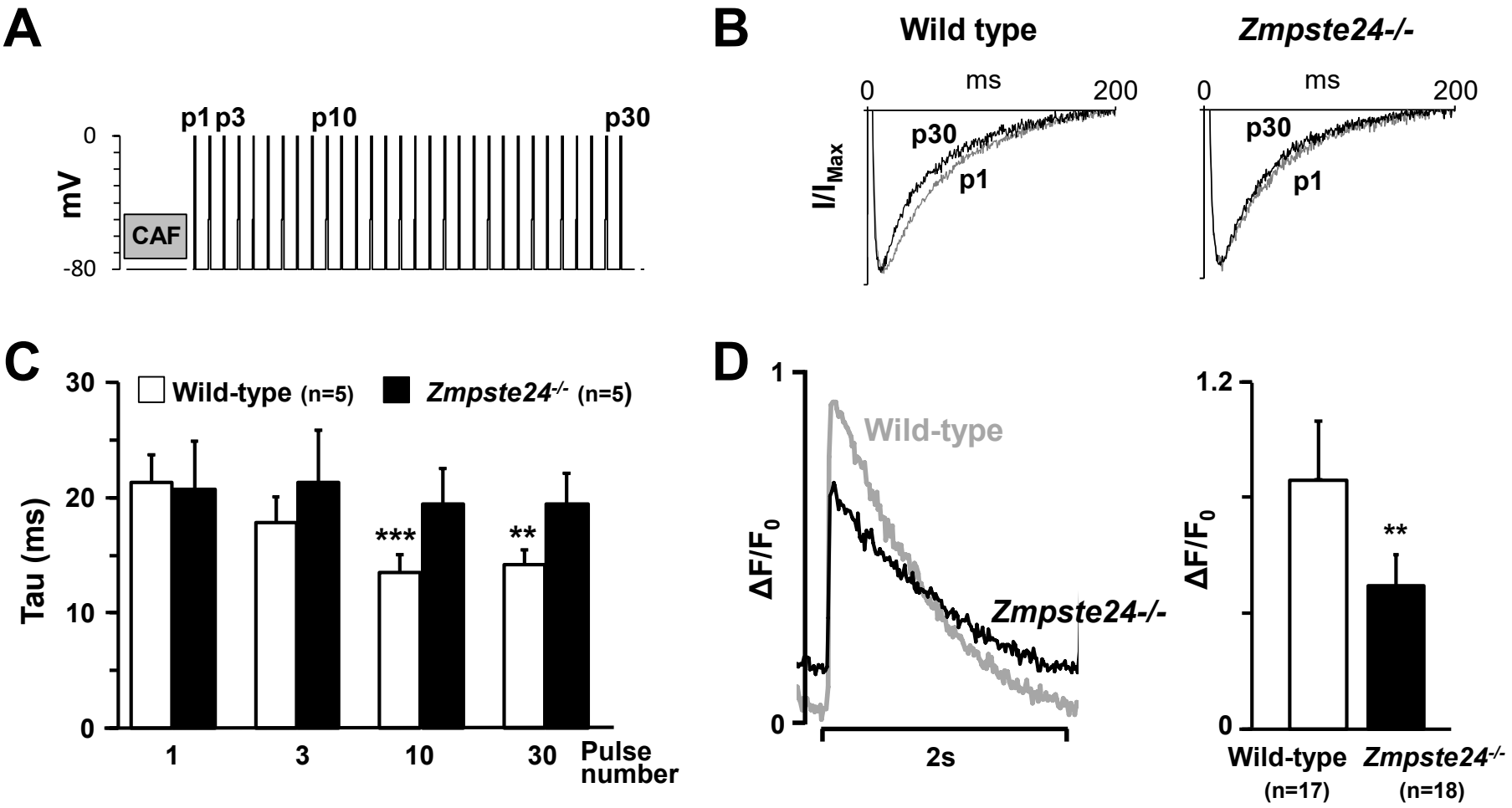
A
p1 p3
p10
p30
0
mV
-80
CAF
B
Wild type
Zmpste24-/-
0
ms
200
p30
p1
I/I_Max
C
Wild-type (n=5)
Zmpste24-/- (n=5)
Tau (ms)
30
20
10
0
***
**
1
3
10
30
Pulse number
D
1
0
Wild-type
Zmpste24-/-
ΔF/F0
2s
1.2
**
Wild-type
(n=17)
Zmpste24-/-
(n=18)

FIGURE 8

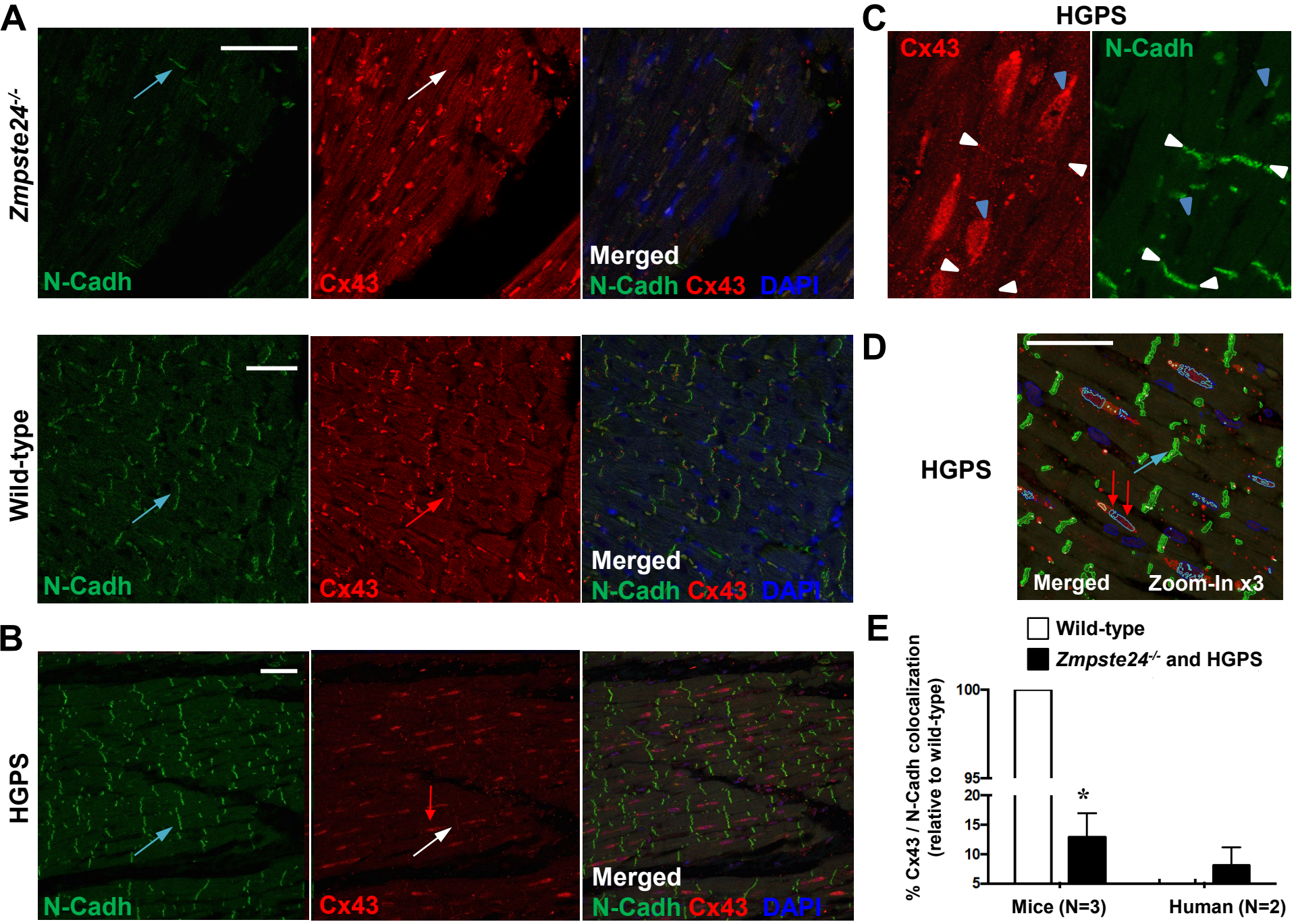
A
Zmpste24-/-
N-Cadh
Cx43
Merged
N-Cadh Cx43 DAPI
Wild-type
N-Cadh
Cx43
Merged
N-Cadh Cx43 DAPI
B
HGPS
N-Cadh
Cx43
Merged
N-Cadh Cx43 DAPI
C
HGPS
Cx43
N-Cadh
D
HGPS
Merged
Zoom-In x3
E
Wild-type
Zmpste24-/- and HGPS
% Cx43 / N-Cadh colocalization
(relative to wild-type)
100
95
20
15
10
5
*
Mice (N=3)
Human (N=2)